DNA-based Signaling Networks for Transient Colloidal Co-Assemblies

Charu Sharma, Avik Samanta, Ricarda Sophia Schmidt, Andreas Walther*

Life-Like Materials and Systems, Department of Chemistry, University of Mainz, Duesbergweg 10-14, 55128 Mainz, Germany.

andreas.walther@uni-mainz.de

Abstract

Programmable chemical circuits inspired by the signaling networks in living cells are a promising approach for the development of adaptive and autonomous self-assembling molecular systems and material functions. Progress has been made at the molecular level, but connecting molecular control circuits to self-assembling larger elements such as colloids that enable real-space studies and access to functional materials is sparse and can suffer from kinetic traps, flocculation, or difficult system integration protocols. Here we report a toehold-mediated DNA strand displacement reaction network capable of autonomously directing two different microgels into transient and self-regulating co-assemblies. The microgels are functionalized with DNA and become elemental components of the network. The flexibility of the circuit design allows the installation of delay phases or accelerators by chaining additional circuit modules upstream or downstream of the core circuit. The design provides an adaptable and robust route to regulate other building blocks for advanced biomimetic functions.

TOC:

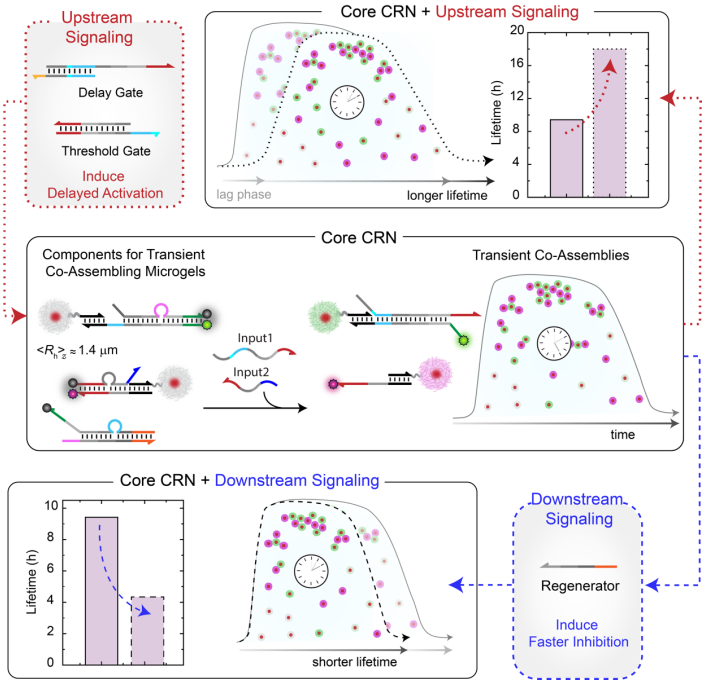

Introduction

In cells, advanced functions such as cell division, motility, motor-mediated organelle transport, and maintenance of cell shape are performed by cytoskeletal structures that exist dynamically in space and time and derive energy for operation from chemical fuel. Depending on the cellular function to be performed, cytoskeletal structures break down and reorganize, changing their life cycles and turnover. At the molecular level, such microscopic functions are regulated by signal transduction from one (upstream) node to another (downstream) in well-defined chemical reaction networks (CRNs), where the signal can be triggered by either extracellular or intracellular events.[1]

Mimicking such dynamic structure formation pathways in a bottom up approach to develop fuel-driven autonomous material systems out-of-equilibrium is an emerging pursuit across the fields of systems chemistry and synthetic biology.[2-4] Diverse building blocks on different length scales like peptides,[5,6] block copolymers,[7] DNA,[8] and nanoparticles[9,10] have been engineered in the recent past for non-equilibrium self-assemblies. Synthetic non-equilibrium self-assembling systems can be realized either by designing the structural elements to be energy dissipating themselves,[11-16] or by coupling responsive structural elements to energy dissipating environments in which the self-assemblies act as a system load to the active environment. Selected examples include pH feedback systems,[17] ATP degradation in ATP-co-assembling systems,[18,19] DNA strand displacement (DSD) circuits,[20-22] Polymerase-Exonuclease-Nickase (PEN) toolbox,[23,24] DNA/RNA genelet circuits,[25-27] and gene regulatory networks.[28,29]

Colloidal nano- and microparticles are versatile building blocks for the development of functional materials, for instance, for applications in photonics and sensing.[30] However, the most challenging task while dealing with colloidal assembly/disassembly is maintaining their overall stability in solution which is usually achieved by balancing van der Waals attraction with electrostatic and steric repulsion. Especially large colloids are prone to excessive flocculation. The integration of colloids with CRNs further requires judicious tuning of activation and deactivation rates to avoid non-dissipative kinetically trapped structures.[11] These limitations explain the scarcity of examples showing autonomous micro(scale) colloidal self-assembly.[9,15,31] Addressing this gap in knowledge, we, for instance, recently coupled pH-responsive microparticles to pH feedback systems to reach transient colloidal co-assembling system featuring a chemo-structural feedback.[9] Dehne et al. showed transient clustering using antagonistic enzymatic reactions of RNA transcription and degradation.[31]

Charting a path forward for autonomous colloidal assemblies requires to think of multicomponent colloidal systems and of chemical circuits with enhanced regulatory capacity. Toehold-mediated DNA strand displacement (TMSD) CRNs exhibit such advantages and feature high programmability, implementation of feedback loops, predictability via computational models, and tunable operational conditions.[32,33] Such TMSD CRNs have previously been exploited for transient self-sorting self-assemblies of DNA origami, or for communication between large coacervate droplets.[20,21] The intermediate colloidal scale remains to be explored. It is relevant because it allows both Brownian dynamics and real space imaging by fluorescence microscopy, and neither the macroscopic droplet system nor the nanoscopic origami system address the challenges regarding colloidal stability.

We herein demonstrate how to integrate a TMSD CRN with colloidal-scale core-shell microgel (MG) particles to autonomously regulate the first transient co-assembly of two building blocks. The particles are elementary components of the TMSD CRN and transduce the input strands with time delays due to the colloidal scale. Due to the versatility of such networks, we show how additional upstream and downstream TMSD modules can be connected to modulate the onset and lifetime of the transient co-assemblies. In addition, the inherent properties of the co-assemblies like assembly size distribution etc., can be regulated temporally. We discuss in detail how to design such CRNs, how to integrate

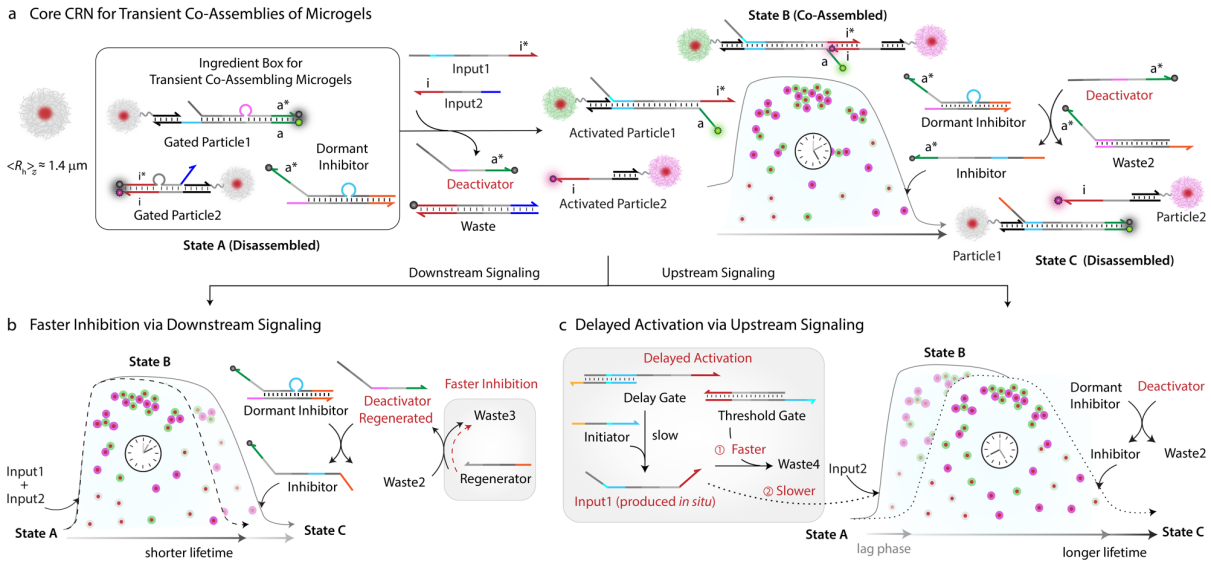

Figure 1. System design for autonomous control of microgel co-assemblies via DNA-based reaction networks. (a) Ingredient box with all the components required to set-up Core CRN. Addition of Input1 and Input2 triggers the transient co-assembly between Particle1 and Particle2. (b) Programming faster inhibition in co-assemblies in response to downstream signaling. (c) Programming the onset time, delay, and an increased lifetime of the co-assemblies by integrating Core CRN with an upstream subnetwork.

upstream and downstream modules, and use simulations and experiments to shed light on details about their operation and coupling to colloidal co-assembly. We envision that our design strategies for building a modular and robust DNA-based CRN with integrable subnetworks can provide a customizable route to regulate the non-equilibrium behavior of other building blocks and ultimately for developing advanced biomimetic functions.

Results and Discussion

System design for the self-regulation of colloidal co-assemblies using modular DNA-based reaction networks.

We use DNA-functionalized micron-sized core-shell MGs as building blocks. Before discussing the rationale behind their use and details of their structure and synthesis, we first introduce the TMSD CRN and its integration with the co-assembling particles, termed Particle1 and Particle2 (Figure 1a). The starting point of the system is a set of gated particles, Gated Particle1 and Gated Particle2, which carry gating modules that prevent assembly in the starting state (State A). The gating modules also carry fluorophore and quencher pairs, and the corresponding fluorescence signals are quenched in State A. The starting mixture also contains a Dormant Inhibitor. Note that all modules carry loops in their structures, which serve as toeholds or energy reservoirs needed to drive the TMSD circuit. Simultaneous addition of Input1 and Input2 to the mixture of Gated Particle1 and Gated Particle2 opens their gates via TMSD and allows them to co-assemble into hetero-complementary structures through interaction of the i/i* domains (State B). The activation can be tracked by the increase of different fluorescent signals (Particle1 turns green; Particle2 turns magenta). While co-assembly takes place, the Deactivator released from the gating module of Gated Particle1 triggers the release of an Inhibitor from the Dormant Inhibitor, present in the medium (shown to the right in Figure 1a). This Inhibitor eventually reacts with the linkage domain between Particle1 and Particle2 (note the “a*” toehold) in the co-assemblies and induces the disassembly of the co-assembled structures (State C). Critically, due to optimization of the sequence space, only the Inhibitor can efficiently break the co-assemblies, whereas other strands containing an a* domain are engineered to be inefficient in this TMSD (see below). Time delays occur due to multivalent binding scenarios and the colloidal nature of

the system. The disassembly leads to a decrease in green fluorescence on Particle1 because the green-labeled strand is hybridized with a quencher labeled Inhibitor during the disassembly process. In contrast, the corresponding magenta fluorescence signal on Particle2 remains unaltered. These processes can be tracked by fluorescence measurements, Confocal Laser Scanning Microscopy (CLSM) and Flow Cytometry.

The modularity of TMSD CRNs allows to increase the regulator capacity of the autonomous system surrounding this Core CRN. We introduce two additional control modules: (1) a downstream accelerator module (Figure 1b), and (2) an upstream signaling module (Figure 1c). For instance, a Regenerator strand, already present in the starting mixture, can recycle the waste produced in the Core CRN and regenerate the Deactivator to increase Inhibitor concentration to accelerate the deactivation and ultimately the disassembly speed (Figure 1b). This leads to shorter lifetimes for State B. Instead of providing Input1 extrinsically to the system, it can be produced *in situ* via an upstream module connected to the Core CRN (Figure 1c). The upstream subnetwork contains a Delay Gate slowly generating Input1 and a Threshold Gate that shares the same sequence as Gated Particle1 but with a longer toehold. The slow production of Input1 and its competitive consumption between Threshold Gate and Gated Particle1 introduces a delay in the activation step. This integration in the Core CRN on a molecular level increases the lifetime of the co-assembled state on a structural level with a pre-defined onset time.

DNA functionalized MGs and their hetero-complementary co-assembly.

Core-shell MGs are our particles of choice as they are well dispersible in aqueous medium and can be functionalized within their shell. The core is composed of a brightly red fluorescent hydrophobic material which is refractive index-matched to water ($\langle R_h \rangle_z \approx 230$ nm, synthesis in Supporting Information section 3.1). The shell contains a lightly crosslinked PNIPAM-*co*-AA hydrogel contributing 90.5 wt% of the MG (80.5 wt% N-isopropylacrylamide (NIPAM); 9 wt% acrylic acid (AA); 1 wt% N,N'-methylenebis(acrylamide) (MBA)). This composition allows functionalization with NH_2-ssDNA (Figure 2a, synthesis in Supporting Information section 3.2). The core-shell MGs have a total $\langle R_h \rangle_z \approx 1.4$ µm and can be well visualized in CLSM (Figure S1). Functionalization by ssDNA can be achieved by EDC-mediated coupling of NH_2-ssDNA (e.g., NH_2-x* and NH_2-z*; EDC = 1-Ethyl-3-(3-dimethylaminopropyl)carbodiimide = 25 equiv. with respect to COOH groups on MG), leading to a typical DNA grafting density of $3.43 \pm 0.03 \times 10^4$ strands per MG or 13.6 ± 0.2 µmol strands per g of MG (Supporting Information section 3.3, Figure S5). Such grafting densities agree with previous literature for DNA-mediated colloidal assembly.[34,35] By using two different NH_2-ssDNA, we prepared a x*-functionalized Particle1 and a z*-functionalized Particle2. The domains x* and z* have no crosstalk to avoid non-specific interactions between Particle1 and Particle2 (NUPACK[36] simulation in Figure S2). Subsequently, we assembled the individual components of the gating modules on each of the particles. For instance, Particle1 was first incubated with equimolar amount of complementary x-P1-Atto488 (4.3 µM), and thereafter with P1*-FQ (4.3 µM; FQ = quencher). The gate on Particle2 (composed of z-P2-Atto647 and P2*-RQ strands) was assembled in a similar way. Step-wise assembly of the gates offers the advantage of visualizing successful functionalization by CLSM as the particles first turn fluorescent, and then the fluorescence is quenched.

The co-assembly activation step by Input addition either introduces (in Gated Particle1) or exposes (in Gated Particle2) a complementary domain i/i* which should bring these particles together into co-assemblies (Figure 2b). We checked for static co-assembly and disassembly with individual components before integrating them into the Core CRN. As expected, an equimolar mixture of Gated Particle1 and Gated Particle2 at a final concentration of 0.05 wt% indeed formed co-assemblies within 2 hours of activation with 4.3 µM each of Input1 and Input2 (2 equiv. with respect to DNA on particles)

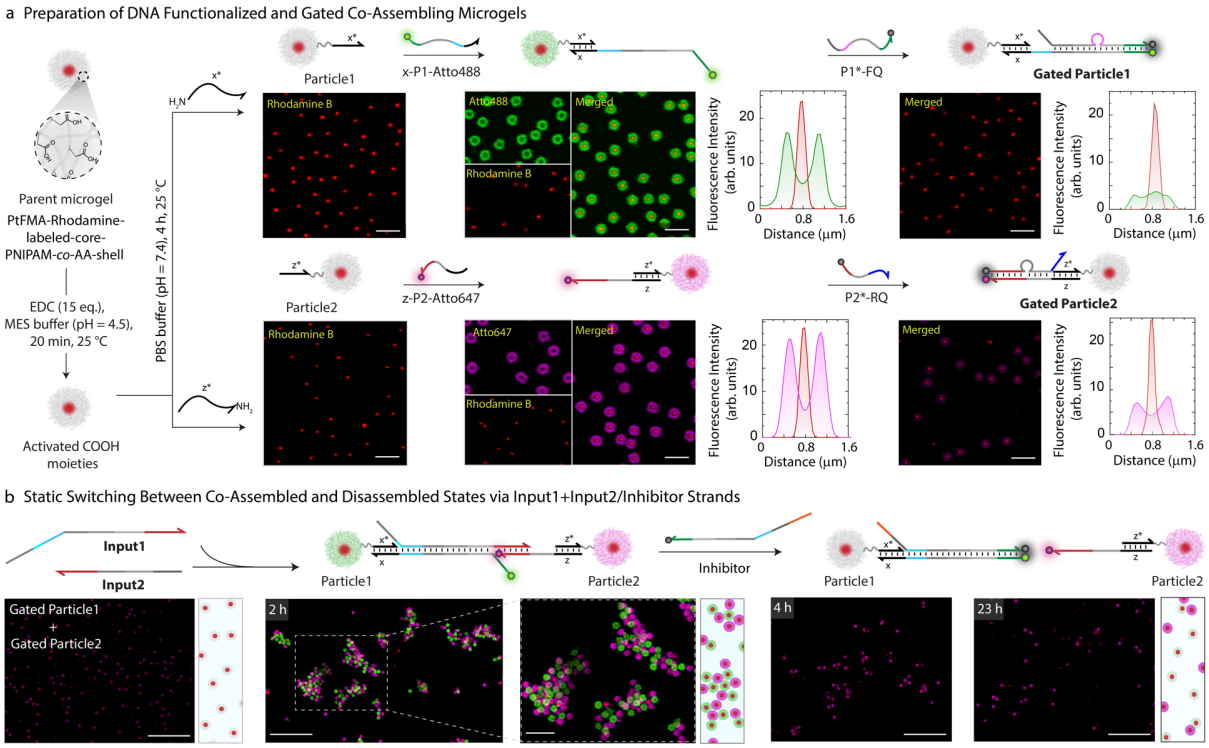

Figure 2. Fabrication and characterization of DNA functionalized co-assembling microgels. (a) Step-wise preparation of a set of Gated Particle1 and Gated Particle2 from a parent microgel. The first step involves covalent functionalization of DNA and consequent annealing with x-P1-Atto488, P1*-FQ on Particle1 and z-P2-Atto647 and P2*-RQ on Particle2. Each step is monitored with CLSM imaging, and the particles are quantitatively analyzed by line segment analysis. Experimental conditions: Particle1 and Particle2 suspended in TE buffer (pH = 8.0) at a final concentration of 0.05 wt%, to which 4.3 μM (1 equiv. with respect to functionalized DNA) of respective annealing strands are added at 15 °C. (b) Monitoring the Gated Particle1 and Gated Particle2 for potential co-assembly by addition of 2 equiv. of Input1 and Input2 and for reversible disassembly by consequent addition of 1 equiv. of Inhibitor. The sample was first checked for co-assembly after 2h of Input addition with *ex situ* CLSM imaging. After addition of Inhibitor strand, sample was again visualized after 4h and 23h. Experimental conditions: Gated Particle1 and Gated Particle2 suspended in TE buffer (pH = 8.0), 50 mM NaCl, 1.5 mM $MgCl_2$ at a final MG concentration of 0.05 wt% at 28 °C. All CLSM images in b are represented as merged composite compiled as a *z*-stack. Scale bars: (a) 2 μm, (b) 10 μm, inset: 3 μm.

as confirmed with CLSM. A subsequent introduction of the Inhibitor displaces Input1 from the co-assemblies, eventually resulting in disassembled particles. The green fluorescent signal on Particle1 is reduced, whereas the magenta signal on Particle2 remains unaltered. This confirms the correct operation of the individual TMSD reactions by the external addition of activating Input and deactivating Inhibitor signals.

Establishing the Core CRN to mediate transient co-assemblies of MGs.

After confirming that particle mixtures can form reversible co-assemblies, we integrated them into the Core CRN. Figure 3a shows this network in greater detail with specific hybridization regions. The system at initial State A contains a stochiometric mixture of Gated Particle1 and Gated Particle2, as well as Dormant Inhibitor in TE buffer (pH = 8.0, 50 mM NaCl, 1.5 mM $MgCl_2$). Simultaneous addition of Input1 and Input2 in equimolar ratio removes the gates on both particles. Input1 displaces the P1-FQ* strand breaking the fluorophore-quencher pair and increasing Atto488 fluorescence on Activated Particle1. Simultaneously, Input2 releases Activated Particle2 from Gated Particle2 and increases Atto647 fluorescence at the shell. During these activation steps, an "i*" domain on Activated Particle1 and a complementary "i" domain on Activated Particle2 are exposed which bind the two particles together via i/i* hybridization. The domain, "i" is designed for a higher binding strength (11 nucleotides (nt), 36.4% CG content, T_m = 30 °C) as compared to other domains used in the CRN. This

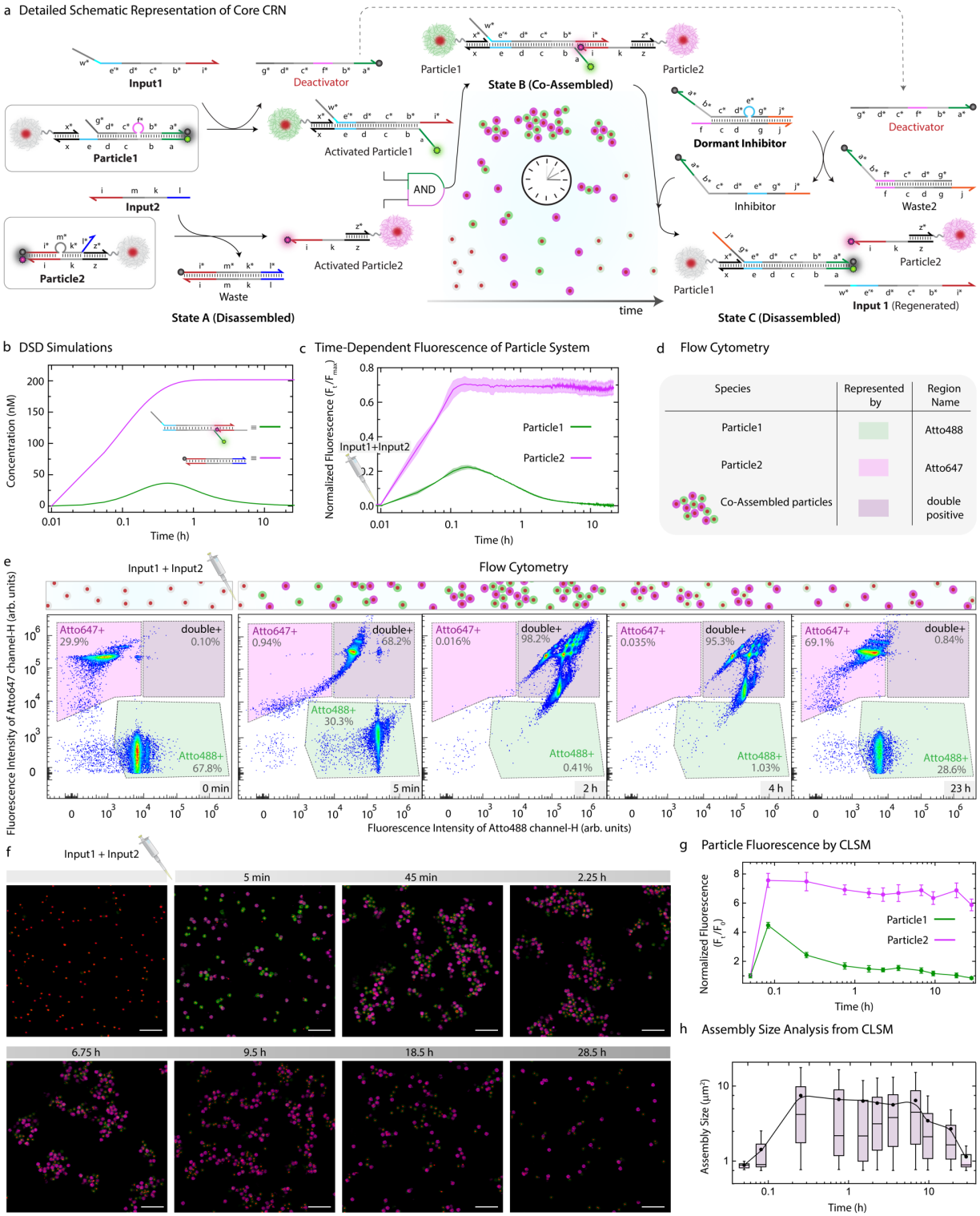

hybridization gradually results in the formation of co-assemblies (State B) owing to multivalent interactions. During the activation of the Gated Particle1, a Deactivator (the P1-FQ* strand) is released which in turn displaces an Inhibitor strand from Dormant Inhibitor by hybridizing to toehold “f” (8 nt). The Inhibitor triggers the negative feedback and breaks the co-assembled complex in the co-assembly by displacing the Input1 strand via toehold “a” (10 nt). This ultimately leads to the disassembly of all particles from the formed co-assemblies. The disassembly step brings the system to a new State C which is marked by the decrease in the Atto488 fluorescence on Particle1 whereas the Atto647 fluorescence on Particle2 remains unaltered. Note that regardless of the complementary toehold “a*” on Dormant Inhibitor and Deactivator, only Inhibitor can energetically favor the disassembly of co-

Figure 3. Core Chemical Reaction Network (Core CRN) used to mediate transient co-assemblies of microgels. (a) Schematic representation of the design and operation of Core CRN. (b) DSD Simulations of the Core CRN predicting the time-dependent behavior of: 1) co-assembled complex (P1-Atto488/Input1/P2-Atto647; green curve), and 2) Waste (Input2/P2*-RQ; magenta curve) produced from the activation step of P2-Atto647/P2*-RQ module. The concentration of the starting modules: P1-Atto488/P1*-FQ, P2-Atto647/P2*-RQ and Dormant Inhibitor is set at 0.25 μM with 2 equiv. of Input1 and Input2. (c) Time-resolved normalized fluorescence of Atto488 and Atto647 dye on Gated Particle1 and Gated Particle2 suspended as equimolar mixture in TE buffer (pH = 8.0), 50 mM NaCl, 1.5 mM $MgCl_2$ at a final MG concentration of 0.005 wt%, 0.25 μM (1 equiv. with respect to DNA gates on particles) of Dormant Inhibitor at 28 °C. The network is initiated with 2 equiv. each of Input1 and Input2. Atto488 and Atto647 fluorescence is normalized with respect to two separate systems containing pre-annealed Activated Particle1 and Activated Particle2 under same experimental conditions. The results represent an average contribution from 2 independent measurements, the shaded region depicts the standard deviation (SD). (d), (e) *ex situ* Flow Cytometric analysis of the Core CRN showing density plots with Atto488 and Atto647 channels on x and y axis respectively where the H denotes the height of the pulse. Three different regions i.e., green, magenta, and purple outlined with dotted boundary represent the gates which are used to isolate Gated Particle1, Gated Particle2 and their co-assembly events respectively from each other. An overhead panel schematically represents the state of the system over the course of experimental investigation. The experiments are performed as described in (c) but at a final MG concentration of 0.05 wt% and 1.5 μM (0.7 equiv.) of Dormant Inhibitor. The network initiated with 2 equiv. each of Input1 and Input2. The aliquots were withdrawn as needed from the reaction mixture and diluted with TE buffer (pH = 8.0) by 100 times before injecting into the Cytometer. (f) *ex situ* CLSM imaging of Core CRN. All CLSM images are represented as merged composite compiled as a *z*-stack. Experimental conditions: same as described in e), aliquots were withdrawn as needed and visualized without any dilution. (g) Fluorescence on Gated Particle1 and Gated Particle2 obtained from CLSM images, each data point represents an average from 15 particles. (h) Assembly size analysis on the particles obtained from two different regions at each time interval. A solid circle represents the mean and horizontal bar the median of the assembly size distribution in box charts. A solid line provides a guide to the eye. Scale bars: 5 μm.

assemblies (Figure S3). The system follows a complex trajectory with a transient state to perform such autonomous functions and overall approaches thermodynamic equilibrium. The energy for the overall execution is supplied by the successive use of toeholds and the opening of bulge loops. In addition, these bulge loops provide steric constraints and protect the toeholds from side reactions during the DSD operation.[37]

To establish and validate the Core CRN design, we performed computer simulations using Visual DSD[38,39] of all modules in absence of the particles (Figure 3b, representative codes are available in Supplementary Notes S2 and S3). The simulations were performed at the same concentrations of DNA modules used for the experiments. The green curve represents the emergence and disappearance of Atto488 fluorescence on Particle1 and corresponds to co-assemblies in state B. The magenta curve represents the expected change in the Atto647 fluorescence during the activation of the gate on Particle2. The simulations clearly show that both particles get activated and that a transient co-assembly is expected. We confirmed these simulations experimentally by time-dependent fluorescence measurements first on free DNA modules, P1-Atto488/P1*-FQ and P2-Atto647/P2*-RQ (Figure S4a) in solution and then on the particle-based system (Figure 3c). Indeed, when the gated particles are treated with both Inputs, the Atto488 fluorescence reaches a transient state (with a maximum yield of 22%) at 11.5 min whereas Atto647 fluorescence saturates to a maximum yield of ~70% within 10.5 min. This confirms the validity of the simulations and hints to a transient self-regulating co-assembly.

CLSM monitoring of the process indeed confirms the transient co-assembly and autonomous operation of the coupled Core CRN/particle system (Figure 3f). Before Input addition, the Gated Particle1 and Gated Particle2 are present in well dispersed state. In a control experiment, no transient co-assemblies are observed in the absence of Input1 and Input2 (Figure S6). After 5 min of Input addition, both particles are activated and form small co-assembled clusters. The average fluorescence intensity on Particle1 increases to ~4.2-fold (green color) and that on Particle2 to ~7.5-fold (magenta color) of their corresponding initial values (Figure 3g). The recorded *z*-stack CLSM images were also

analyzed quantitatively for their change in assembly size over time (Figure 3h). The fluorescence intensity on Particle1 already starts to decrease after 5 min whereas that on Particle2 reaches a plateau. The size of the co-assemblies however continues to increase as suggested by assembly size distribution analysis which reaches a maximum value after 15 min and stays the same until 6.75 h. After 7 h, the structures begin to disassemble and dissolve completely after 28 h.

To further quantify the behavior on a population ensemble level, we used flow cytometry that is able to identify particle species according to their fluorescence and the state of assembly according to their scattering (Figure 3d,e). We injected aliquots of an autonomously developing particle co-assembly system into the cytometer at different time intervals after Input addition (5 min, 2 h, 4 h, and 23 h). At 0 min, Particle1 and Particle2 can be clearly identified in their regions. 5 minutes after addition of Input1 and Input2, majorly two distinct populations of Particle1 and Particle2 can still be observed, but they exhibit a higher fluorescence intensity originating from an increased activation by removing the respective quencher strands. This is consistent with the fluorescence increase observed in solution spectroscopic analysis (Figure 3c). The subsequent co-assembly is evident at 2 h, as the two distinct populations of Particle1 and Particle2 merge into the double positive area (98% of all particles). Interestingly, the observation of distinct patterns in the co-assembly population indicates the presence of co-assemblies with gradual increase in particle numbers (see Figure S7, S8, Supplementary Note S8 for details). After 4 h, degradation of the co-assembly occurs, as the population in the double positive region starts to decrease. Complete degradation of the co-assembled state and return of the system to the initial state (dispersed population) is observed after 23 h. The populations also show that the Atto488 fluorescence (Particle1) returns to its quenched state, while the Atto647 fluorescence (Particle2) remains in its activated state. Again, this conforms to expectations of the CRN and to the fluorescence spectroscopic measurements (Figure 3c). The consistent evolution of cytometry data underscores the transient co-assemblies triggered by the CRN and confirms the robustness of our design.

Faster inhibition of co-assemblies by installing a downstream signaling module.

After successfully establishing the Core CRN/particle system, we wondered if we could modulate the kinetics and size of the co-assemblies in response to an additional external signal. Specifically, could we accelerate the destruction of the co-assemblies and decrease the overall lifetime of the co-assemblies? To achieve this, we developed a Regenerator strand (1 equiv. with respect to Gated Particle1 and Gated Particle2) that regenerates the Deactivator from Waste2. Overall, no extra waste is produced in the process, old waste (Waste2) is recycled to generate Waste3 (Figure 4a). Simulations suggest that the co-assembled complex in the presence of Regenerator disassembles faster whereas the activation on Particle2 shows no change (see change to dotted green line in Figure 4b, Supplementary Notes S4 and S5). In the Core CRN, the Inhibitor is produced following a slight lag from the Deactivator generation (Figure S10) and the co-assembled complex starts to dissociate once the Inhibitor acquires a threshold yield of 7% at 14 min. However, in the presence of Regenerator, the Inhibitor reaches the same threshold within 8 min (Figure S10). This leads to an earlier dissociation of the co-assembled complex.

Fluorescence profiles of free DNA modules, P1-Atto488/P1*-FQ and P2-Atto647/P2*-RQ in the presence of a Regenerator agree with the simulations (Figure S3b). When implemented with the particle system, a similar trend of faster inhibition in the Atto488 fluorescence on Gated Particle1 is observed (green line in Figure 4c). The Atto647 fluorescence on Gated Particle2 levels off at 65% yield within 30 min (magenta line in Figure 4c). The Atto647 fluorescence in presence of a Regenerator shows a slight delay regarding its increase as compared to the Core CRN without Regenerator (dotted vs solid magenta line in Figure 4c). This should however not be overinterpreted on this part of the

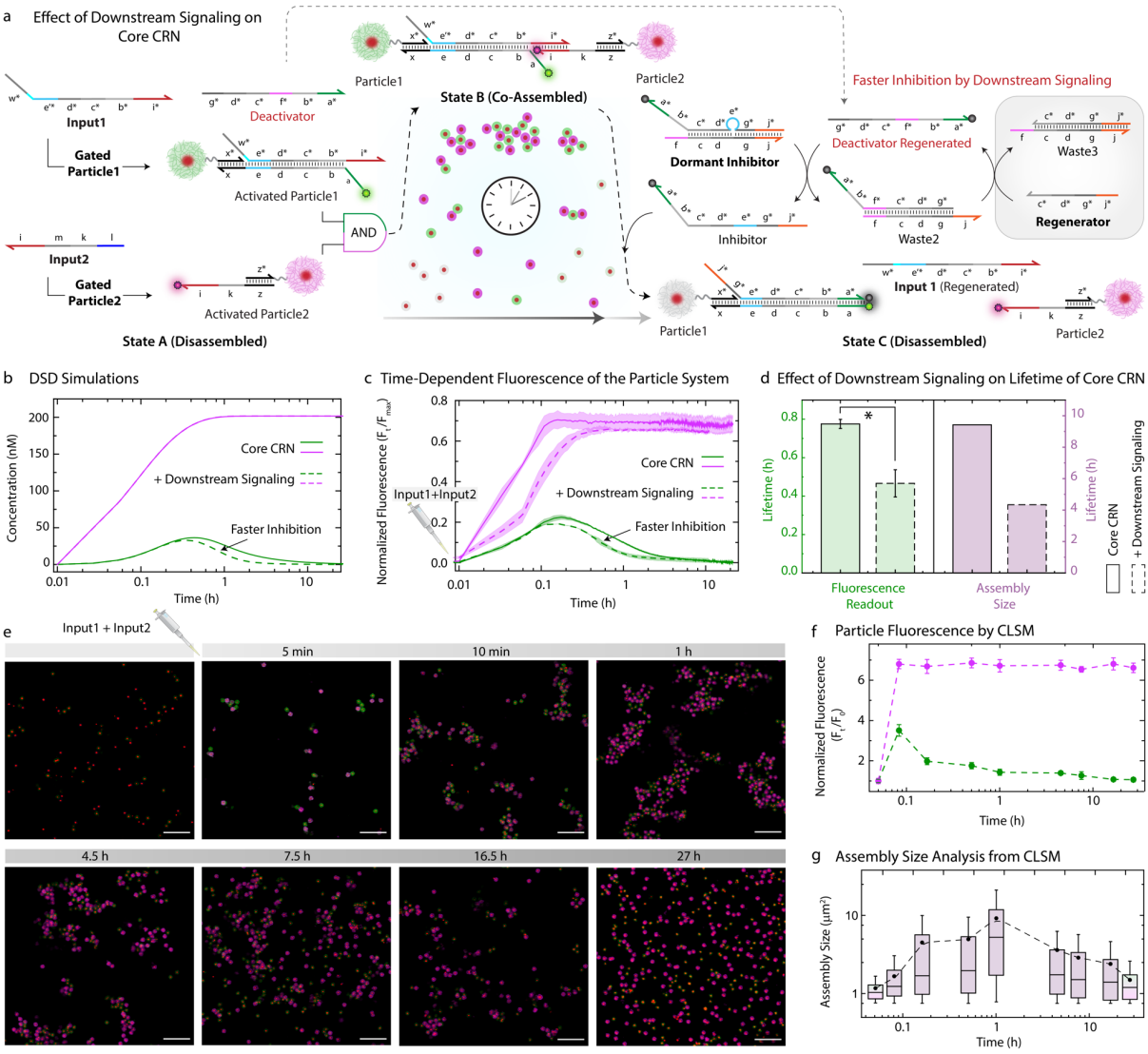

Figure 4. Effect of faster inhibition on Core CRN via downstream signaling. (a) Schematic representation of the design and operation of Core CRN in the presence of a downstream module consisting of Regenerator. (b) DSD Simulations predicting the behavior of co-assembled complex (green curve) and Waste (magenta curve), the effect of a Regenerator is represented by dashed curves. The concentration of both modules is set at 0.25 μM with 0.25 μM of Dormant Inhibitor, Regenerator and 2 equiv. each of Input1 and Input2. (c) Time-resolved normalized fluorescence of Atto488 and Atto647 dye on Particle1 and Particle2 suspended as equimolar mixture in TE buffer (pH = 8.0), 50 mM NaCl, 1.5 mM $MgCl_2$ at a final MG concentration of 0.005 wt%, 0.25 μM (1 equiv.) Dormant Inhibitor and, 0.25 μM (1 equiv.) Regenerator at 28 °C. The network is initiated with 2 equiv. each of Input1 and Input2. The effect of Regenerator strand is plotted with dashed lines. Atto488 and Atto647 fluorescence is normalized with respect to two separate systems containing pre-annealed Activated Particle1 and Activated Particle2 under same experimental conditions. The results represent an average contribution from 2 independent measurements, the shaded region depicts the SD. (d) The lifetime comparison of the transient state obtained from time-dependent fluorescence measurements, size distribution analysis and particle fluorescence from *ex situ* CLSM between Core CRN with (bars with dashed boundaries) and without (bars with solid boundaries) downstream signaling. * indicate that $p < 0.05$. (e) *ex situ* CLSM imaging of Core CRN in the presence of Regenerator. All CLSM images are represented as merged composite compiled as a *z*-stack. Experimental conditions: same as described in (c) but at a final MG concentration of 0.05 wt%, 1.5 μM (0.7 equiv.) of Dormant Inhibitor and Regenerator strand at 28 °C. The network is initiated with 2 equiv. each of Input1 and Input2. Aliquots were withdrawn as needed and visualized without any dilution. (f) Fluorescence on Gated Particle1 and Gated Particle2 obtained from CLSM images, each data point represents an average from 15 particles. (g) Assembly size analysis on the particles obtained from two different *z*-stacks at each time interval. A solid circle represents the mean and horizontal bar the median of the assembly size distribution in box charts. A dashed line provides a guide to the eye. Scale bars: 5 μm.

logarithmic scale, and critically, the overall faster inhibition is well reflected in the spectroscopic

analysis (dotted vs solid green line in Figure 4c).

The transient profiles can be easily compared through their lifetimes, which is the time period that the fluorescence profile takes to decrease to the level corresponding to the half of the initial and the maximum fluorescence. As anticipated, the lifetime of the fluorescence profile corresponding to the Activated Particles in Core CRN (~46.2 min) can be reduced by 1.7 times in the presence of downstream signaling (~27.6 min) (Figure 4d).

To check whether the shorter lifetime observed in the fluorescence profiles can be translated for reduced lifetime of the co-assembled structures, we monitored the system via CLSM (Figure 4e). Without Input addition, Gated Particle1 and Gated Particle2 continue to remain well dispersed and inactivated until 48h (Figure S8). Within only 5 minutes of Input 1 and 2 addition, Particle1 and Particle2 are activated (Figure 4f). But this time, Atto488 fluorescence on Particle1 increases to only 3.5 times of its initial value compared to 4.2 times increase in case of Core CRN. This is to be expected according to the simulations: Faster inhibition in the presence of Regenerator compromises the overall yield of activated modules (x-P1-Atto488/Input1) on Particle1. The increase in the Atto647 fluorescence on Particle2 however remains the same (~7 times). The activation thereby triggers co-assembly of Particle1 and Particle2 reaching their maximum size (10 μm^2) slowly after 1 h (Figure 4g). The structures start to disassemble soon after that, with a lifetime of only ~4 h compared to the Core CRN without Regenerator (~9 h). The reduced lifetime confirms the faster destruction of the co-assembled structures in the presence of Regenerator. The above results validate the robustness of the Core CRN even when integrated with downstream signal. The shorter lifetime of the co-assembled structures proves that a simple change in the network can bring out advance changes on the system level without hampering the overall performance of the original network.

Introduction of a delay and threshold for co-assembly via an upstream signaling module.

Next, we asked whether we can further modulate the Core CRN to process a signal wired through upstream reactions to induce a programmed delay time with a signal thresholding function into the lifecycle. To demonstrate the concept, we first designed a Delay Gate bearing a toehold containing only 3 nt (CTC) through which Input1 is generated upon addition of an Initiator (Figure 5a). Under the same conditions, reactions mediated by 3 nt toeholds proceed approximately 10-100 times slower than 7-8 nt long toeholds which are used in other parts of the CRN.[40] In most cellular processes, an output is generated when the input concentration reaches above a threshold concentration which creates a presence/absence interpretation associated with the thresholding unit.[41] Thresholding can be adapted in TMSD by designing a Threshold Gate to possess a longer toehold than the competing target gate such that the incoming Input is preferentially consumed by the Threshold Gate, only after which the Input becomes available for target gate on Gated Particle1.[42,43]

Without making any amendments in the Core CRN, we built a Threshold Gate that shares the same sequence as the P1-Atto488/P1*-FQ module on Gated Particle 1 (toehold sequence, e = GTGTAATA, k_b ≈ 3.3 X 10^{-6} $nM^{-1}s^{-1}$) but with a longer toehold containing 3 extra nt (TCC) at the end (toehold sequence at Threshold Gate, e´ = GTGTAATATCC, k_b ≈ 7 X 10^{-6} $nM^{-1}s^{-1}$). In this case, it is not the increase in the toehold length alone (from 8 to 11 nt), but the 15% increase in the overall G-C content (25% for "e" and 40% for "e´") which allows the Input1 to react with Threshold Gate ~2 times faster than the P1-Atto488/P1*-FQ module.[40] Simulations confirm that there is a strong competition between the reaction of Input1 with Threshold Gate versus P1-Atto488/P1*-FQ module where both of them follow two-phase exponential decay (Figure S13). As anticipated, the rate of consumption or the decay rate of Threshold Gate ($k_{decay,Threshold\ Gate}$ ≈ 1.4 h^{-1}) is higher than that of P1-Atto488/P1*-FQ module ($k_{decay,P1/P1*}$ ≈ 0.9 h^{-1}). The combined effect of (i) slow *in situ* production of Input1

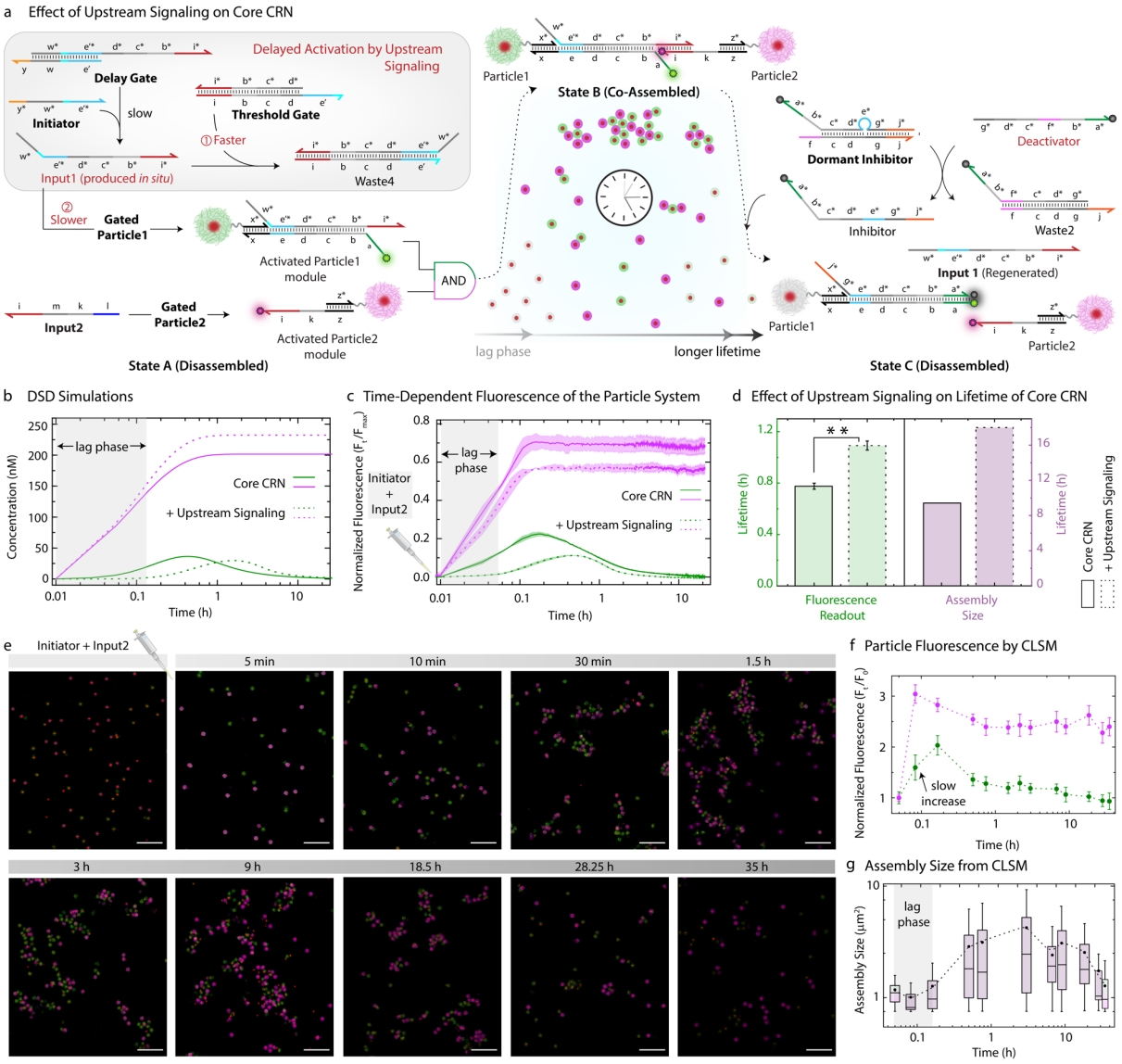

Figure 5. Effect of delayed activation on Core CRN via upstream signaling. (a) Schematic representation of the design and operation of Core CRN in the presence of an upstream module consisting of a Delay Gate and a Threshold Gate. The concentration of both modules is set at 0.25 μM with 0.25 μM of Dormant Inhibitor, Threshold Gate, 0.5 μM of Delay Gate, 4 equiv. of Initiator and 2 equiv. of Input2. (b) DSD Simulations predicting the behavior of co-assembled complex (green curve) and Waste (magenta curve), the effect of upstream module is represented by dotted curves. (c) Time-resolved normalized fluorescence of Atto488 and Atto647 dye on Particle1 and Particle2 suspended as equimolar mixture in TE buffer (pH = 8.0), 50 mM NaCl, 1.5 mM $MgCl_2$ at a final MG concentration of 0.005 wt%, 0.25 μM (1 equiv.) Dormant Inhibitor, 0.25 μM (1 equiv.) Threshold Gate, 0.5 μM (2 equiv.) Delay Gate at 28 °C. The network is initiated with 4 equiv. of Initiator and 2 equiv. of Input2. The effect of upstream module is plotted with dotted lines. Atto488 and Atto647 fluorescence is normalized with respect to two separate systems containing pre-annealed Activated Particle1 and Activated Particle2 under same experimental conditions. The results represent an average contribution from 2 independent measurements, the shaded region depicts the SD. (d) The lifetime comparison of the transient state obtained from time-dependent fluorescence measurements, area distribution analysis and line segment analysis from *ex situ* CLSM between Core CRN with (bars with dotted boundaries) and without (bars with solid boundaries) upstream signaling. ** indicate that $p < 0.01$. (e) *ex situ* CLSM measurements of Core CRN integrated with upstream signaling. All CLSM images are represented as merged composite compiled as a *z*-stack. Experimental conditions: same as described in c) but at a final MG concentration of 0.05 wt%, 1.5 μM (0.7 equiv.) Dormant Inhibitor, 1.5 μM (0.7 equiv.) Threshold Gate, 3 μM (1.4 equiv.) Delay Gate at 28 °C. The network is initiated with 4 equiv. of Initiator and 2 equiv. of Input2. Aliquots were withdrawn as needed and visualized without any dilution. (f) Fluorescence on Gated Particle1 and Gated Particle2 obtained from CLSM images, each data point represents an average from 15 particles. (g) Assembly size analysis on the particles obtained from two different *z*-stacks at each time interval. A solid circle represents the mean and horizontal bar the median of the assembly size distribution in box charts. A dotted line provides a guide to the eye. Scale bars: 5 μm.

through a Delay Gate based on adding the Initiator and (ii) a subsequent competition for Input1 between Threshold Gate versus P1-Atto488 /P1*-FQ module generates a well-defined lag time of ~5 min as determined from simulations (Figure 5b, Supplementary Notes S6 and S7). Moreover, an overall delay of ~1 h is expected for the Atto488 fluorescence to achieve its maximum yield of 12%. Experimentally, the lag phase and an associated delay in Atto488 fluorescence from Atto488-P1 is confirmed with time-dependent fluorescence measurement on free DNA modules (Figure S3c).

Similar fluorescence trends are observed when the system is implemented with the particles (Figure 5b). Upon simultaneous addition of Initiator and Input2, activation on Particle1 is observed after a well-defined lag of ~4 min with a jump in the lifetime from 0.77 h to 1.09 h (Figure 5c,d). Atto647 fluorescence on Particle2 reaches its saturated state within ~ 4 min, similar to that observed in the absence of upstream signaling, but with a reduced yield of 60% which can be explained because of local fluctuations in the environment of the fluorophore. The observed trend in the Atto488 and Atto647 fluorescence confirms the efficiency of the Core CRN in the presence of an upstream module. This lag time and delay come however on the expense of reduced activation on Particle1 and Particle2.

To check whether 11% maximum yield (only half of the original network, 22%) of the activated Particle1 is sufficient to induce co-assemblies, we performed CLSM experiments. The gated particles stay inactivated and well dispersed before providing any Initiator and Input2 (Figure S11). However, upon simultaneous addition of Initiator and Input2 to an equimolar mixture of Gated Particle1 and Gated Particle2, a ~3-fold increase in the Atto647 fluorescence on the Particle2 is observed within 5 min (Figure 5e). Atto488 fluorescence on Particle1 increases to 2 times of its initial value, which is only half the increase observed in Core CRN (4.3 times increase) after 10 min (Figure 5f). The slow increase and the low yield of activation of Particle1 gate does not induce any co-assemblies within 10 min, unlike for the Core CRN/particle system (Figure 5g, 3 h). However, after 30 min, the co-assembled structures are finally observed and gradually grow in size and reach their maximum average size of 8 μm^2 after 3 h. The overall time taken by the co-assemblies to reach their maximum average size is delayed by 2.75 h with a relative decrease of 2 μm^2 in the average size of the co-assemblies. The relatively less activated strands on Particle1 and Particle2 reduce the multivalency strength for co-assembly and thereby explain the reduced co-assembly size. Beyond this point, Atto488 fluorescence on Particle1 continues to decrease, and the co-assembled structures slowly begin to disassemble and complete disassembly is only observed after 35 h. It is important to note that the relatively slow production of Input1 in this case also slows down the Deactivator and hence the Inhibitor generation in the downstream processes. This directly influences the disassembly step, which increases the lifetime of the transient co-assembled state from 9.42 to 18 h (Figure 5d).

Discussion

In this work, we presented the first example of a transient co-assembling system that uses micron-scale soft colloids as primary building blocks carrying molecular information relays for signal acquisition, processing, and transduction through a series of concatenated TMSD reactions. Our approach combines the concepts of polymer chemistry in the form of the design and synthesis of DNA-decorated monodisperse microgels with a cornerstone of dynamic DNA nanotechnology in the form of TMSD-based CRNs that enable rational design of signaling and feedback loops. The micrometer-sized building blocks facilitate distinction and monitoring of the transient assembly process by CLSM and Flow Cytometry.

Owing to the versatility and programmability of the TMSD-based CRN, the lifetime of the co-assembled state could be shortened by amplifying the negative feedback through the addition of a Regenerator or extended by delaying the activation signal through the introduction of a Threshold and

Delay Gate. In addition, *in silico* optimization of DNA modules provides essential guidance for experimental design and analysis. Next to the temporal property of the DSD circuits, we designed our two populations of microgel particles carrying the respective modules in a way that two distinct fluorescence signals emanate from each population over the course of the CRN. The distinguishability of the particle populations allows us not only to monitor the transient pathway of co-assemblies using CLSM and cytometric analysis but also to quantify the respective size distribution of the resulting co-assemblies. It also allows to link molecular activation/deactivation reactions to colloidal scale processes that experience obvious delays. Our optimized DNA sequences for the Core CRN operate smoothly and confirm our expectations despite the spatial confinement and steric factors associated with immobilized DNA on the microgel surface. Moreover, the programmability of the TMSD reactions also provides the opportunity to optimize the transient self-assembly systems to avoid non-dissipative, kinetically trapped aggregates by simply changing the binding strength and nucleotide composition of the toeholds and other domains.

The TMSD circuit demonstrated here in the microparticle systems provides a starting point to extend the system engineering to more sophisticated systems, such as ATP-driven TMSD circuits,[44] catalytic TMSD circuits,[45] or even the inclusion of additional functions that arise in the co-assembled state of the microparticles. The energy stored in such dissipative non-equilibrium assemblies can be further transduced into mechanical energy to achieve advanced functions such as shape-change control/maintenance and movement.[46] The size of these particles allows their exploitation for designing interactive materials for photonics, sensors, and delivery systems applications. In fact, the sensing and processing properties of these particles demonstrated in this study can be an essential parameter for communication with living cells leading to bioactive materials.[47]

References

1. Nussinov, R., Tsai, C.-J., and Jang, H. (2022). Allostery, and how to define and measure signal transduction. Biophys. Chem. *283*, 106766. https://doi.org/10.1016/j.bpc.2022.106766.
2. della Sala, F., Neri, S., Maiti, S., Chen, J.L.Y., and Prins, L.J. (2017). Transient self-assembly of molecular nanostructures driven by chemical fuels. Curr. Opin. Biotechnol. *46*, 27-33. https://doi.org/10.1016/j.copbio.2016.10.014.
3. van Ravensteijn, B.G.P., Voets, I.K., Kegel, W.K., and Eelkema, R. (2020). Out-of-Equilibrium Colloidal Assembly Driven by Chemical Reaction Networks. Langmuir *36*, 10639-10656. 10.1021/acs.langmuir.0c01763.
4. Walther, A. (2020). Viewpoint: From Responsive to Adaptive and Interactive Materials and Materials Systems: A Roadmap. Adv. Mater. *32*, 1905111. https://doi.org/10.1002/adma.201905111.
5. Levin, A., Hakala, T.A., Schnaider, L., Bernardes, G.J.L., Gazit, E., and Knowles, T.P.J. (2020). Biomimetic peptide self-assembly for functional materials. Nat. Revi. Chem. *4*, 615-634. 10.1038/s41570-020-0215-y.
6. Heuser, T., Steppert, A.K., Lopez, C.M., Zhu, B., and Walther, A. (2015). Generic concept to program the time domain of self-assemblies with a self-regulation mechanism. Nano Lett. *15*, 2213-2219. 10.1021/nl5039506.
7. Cingil, H.E., Meertens, N.C.H., and Voets, I.K. (2018). Temporally Programmed Disassembly and Reassembly of C3Ms. Small *14*, e1802089. 10.1002/smll.201802089.
8. Heinen, L., and Walther, A. (2017). Temporal control of i-motif switch lifetimes for autonomous operation of transient DNA nanostructures. Chem. Sci. *8*, 4100-4107. 10.1039/c7sc00646b.

9. Sharma, C., and Walther, A. (2022). Self-Regulating Colloidal Co-Assemblies That Accelerate Their Own Destruction via Chemo-Structural Feedback. Angew. Chem. Int. Ed. *61*, e202201573. https://doi.org/10.1002/anie.202201573.
10. Laramy, C.R., O'Brien, M.N., and Mirkin, C.A. (2019). Crystal engineering with DNA. Nat. Rev. Mater. *4*, 201-224. 10.1038/s41578-019-0087-2.
11. Merindol, R., and Walther, A. (2017). Materials learning from life: concepts for active, adaptive and autonomous molecular systems. Chem. Soc. Rev. *46*, 5588-5619. 10.1039/C6CS00738D.
12. Schwarz, P.S., Tena-Solsona, M., Dai, K., and Boekhoven, J. (2022). Carbodiimide-fueled catalytic reaction cycles to regulate supramolecular processes. Chem. Commun. *58*, 1284-1297. 10.1039/d1cc06428b.
13. Boekhoven, J., Hendriksen, W.E., Koper, G.J., Eelkema, R., and van Esch, J.H. (2015). Transient assembly of active materials fueled by a chemical reaction. Science *349*, 1075-1079. 10.1126/science.aac6103.
14. Heinen, L., and Walther, A. (2019). Programmable dynamic steady states in ATP-driven nonequilibrium DNA systems. Sci. Adv. *5*, eaaw0590. 10.1126/sciadv.aaw0590.
15. Deng, J., and Walther, A. (2020). ATP-powered molecular recognition to engineer transient multivalency and self-sorting 4D hierarchical systems. Nat. Commun. *11*, 3658. 10.1038/s41467-020-17479-9.
16. Deng, J., and Walther, A. (2021). Autonomous DNA nanostructures instructed by hierarchically concatenated chemical reaction networks. Nat. Commun. *12*, 5132. 10.1038/s41467-021-25450-5.
17. Sharma, C., Maity, I., and Walther, A. (2023). pH-feedback systems to program autonomous self-assembly and material lifecycles. Chem. Commun. *59*, 1125-1144. 10.1039/D2CC06402B.
18. Maiti, S., Fortunati, I., Ferrante, C., Scrimin, P., and Prins, L.J. (2016). Dissipative self-assembly of vesicular nanoreactors. Nat. Chem. *8*, 725-731. 10.1038/nchem.2511.
19. Mishra, A., Dhiman, S., and George, S.J. (2021). ATP-Driven Synthetic Supramolecular Assemblies: From ATP as a Template to Fuel. Angew. Chem. Int. Ed. *60*, 2740-2756. 10.1002/anie.202006614.
20. Joesaar, A., Yang, S., Bogels, B., van der Linden, A., Pieters, P., Kumar, B., Dalchau, N., Phillips, A., Mann, S., and de Greef, T.F.A. (2019). DNA-based communication in populations of synthetic protocells. Nat. Nanotechnol. *14*, 369-378. 10.1038/s41565-019-0399-9.
21. Groeer, S., Schumann, K., Loescher, S., and Walther, A. (2021). Molecular communication relays for dynamic cross-regulation of self-sorting fibrillar self-assemblies. Sci. Adv. *7*, eabj5827. doi:10.1126/sciadv.abj5827.
22. Srinivas, N., Parkin, J., Seelig, G., Winfree, E., and Soloveichik, D. (2017). Enzyme-free nucleic acid dynamical systems. Science *358*, eaal2052. doi:10.1126/science.aal2052.
23. Gines, G., Zadorin, A.S., Galas, J.C., Fujii, T., Estevez-Torres, A., and Rondelez, Y. (2017). Microscopic agents programmed by DNA circuits. Nat. Nanotechnol. *12*, 351-359. 10.1038/nnano.2016.299.
24. Zambrano, A., Fracasso, G., Gao, M., Ugrinic, M., Wang, D., Appelhans, D., deMello, A., and Tang, T.Y.D. (2022). Programmable synthetic cell networks regulated by tuneable reaction rates. Nat. Commun. *13*, 3885. 10.1038/s41467-022-31471-5.
25. Qin, Z., Liu, Y., Zhang, L., Liu, J., and Su, X. (2022). Programming Dissipation Systems by DNA Timer for Temporally Regulating Enzyme Catalysis and Nanostructure Assembly. ACS Nano *16*, 14274-14283. 10.1021/acsnano.2c04405.
26. Green, L.N., Subramanian, H.K.K., Mardanlou, V., Kim, J., Hariadi, R.F., and Franco, E. (2019). Autonomous dynamic control of DNA nanostructure self-assembly. Nat. Chem. *11*, 510-520. 10.1038/s41557-019-0251-8.
27. Gentile, S., Del Grosso, E., Pungchai, P.E., Franco, E., Prins, L.J., and Ricci, F. (2021). Spontaneous Reorganization of DNA-Based Polymers in Higher Ordered Structures Fueled by RNA. J. Am. Chem. Soc. *143*, 20296-20301. 10.1021/jacs.1c09503.

28. Schaffter, S.W., and Schulman, R. (2019). Building in vitro transcriptional regulatory networks by successively integrating multiple functional circuit modules. Nat. Chem. *11*, 829-838. 10.1038/s41557-019-0292-z.
29. Dupin, A., and Simmel, F.C. (2019). Signalling and differentiation in emulsion-based multi-compartmentalized in vitro gene circuits. Nat. Chem. *11*, 32-39. 10.1038/s41557-018-0174-9.
30. Cai, Z., Li, Z., Ravaine, S., He, M., Song, Y., Yin, Y., Zheng, H., Teng, J., and Zhang, A. (2021). From colloidal particles to photonic crystals: advances in self-assembly and their emerging applications. Chem. Soc. Rev. *50*, 5898-5951. 10.1039/D0CS00706D.
31. Dehne, H., Reitenbach, A., and Bausch, A.R. (2019). Transient self-organisation of DNA coated colloids directed by enzymatic reactions. Sci. Rep. *9*, 7350. 10.1038/s41598-019-43720-7.
32. Dalchau, N., Szép, G., Hernansaiz-Ballesteros, R., Barnes, C.P., Cardelli, L., Phillips, A., and Csikász-Nagy, A. (2018). Computing with biological switches and clocks. Nat Comput *17*, 761-779. 10.1007/s11047-018-9686-x.
33. Seeman, N.C. (2003). DNA in a material world. Nature *421*, 427-431. 10.1038/nature01406.
34. Wang, Y., Wang, Y., Zheng, X., Ducrot, É., Lee, M.-G., Yi, G.-R., Weck, M., and Pine, D.J. (2015). Synthetic Strategies Toward DNA-Coated Colloids that Crystallize. J. Am. Chem. Soc. *137*, 10760-10766. 10.1021/jacs.5b06607.
35. Hennig, A., Borcherding, H., Jaeger, C., Hatami, S., Würth, C., Hoffmann, A., Hoffmann, K., Thiele, T., Schedler, U., and Resch-Genger, U. (2012). Scope and Limitations of Surface Functional Group Quantification Methods: Exploratory Study with Poly(acrylic acid)-Grafted Micro- and Nanoparticles. J. Am. Chem. Soc. *134*, 8268-8276. 10.1021/ja302649g.
36. Zadeh, J.N., Steenberg, C.D., Bois, J.S., Wolfe, B.R., Pierce, M.B., Khan, A.R., Dirks, R.M., and Pierce, N.A. (2011). NUPACK: Analysis and design of nucleic acid systems. J. Comput. Chem. *32*, 170-173. 10.1002/jcc.21596.
37. Sullivan, R., Adams, M.C., Naik, R.R., and Milam, V.T. (2019). Analyzing Secondary Structure Patterns in DNA Aptamers Identified via CompELS. Molecules *24*, 1572.
38. Lakin, M.R., Youssef, S., Polo, F., Emmott, S., and Phillips, A. (2011). Visual DSD: a design and analysis tool for DNA strand displacement systems. Bioinformatics *27*, 3211-3213. 10.1093/bioinformatics/btr543.
39. Petersen, R.L., Lakin, M.R., and Phillips, A. (2016). A strand graph semantics for DNA-based computation. Theor. Comput. Sci. *632*, 43-73. 10.1016/j.tcs.2015.07.041.
40. Zhang, D.Y., and Winfree, E. (2009). Control of DNA Strand Displacement Kinetics Using Toehold Exchange. J. Am. Chem. Soc. *131*, 17303-17314. 10.1021/ja906987s.
41. Mannan, A.A., Liu, D., Zhang, F., and Oyarzún, D.A. (2017). Fundamental Design Principles for Transcription-Factor-Based Metabolite Biosensors. ACS Synth. Biol. *6*, 1851-1859. 10.1021/acssynbio.7b00172.
42. Qian, L., Winfree, E., and Bruck, J. (2011). Neural network computation with DNA strand displacement cascades. Nature *475*, 368-372. 10.1038/nature10262.
43. Jung, J.K., Archuleta, C.M., Alam, K.K., and Lucks, J.B. (2022). Programming cell-free biosensors with DNA strand displacement circuits. Nat. Chem. Biol. *18*, 385-393. 10.1038/s41589-021-00962-9.
44. Deng, J., and Walther, A. (2020). Fuel-Driven Transient DNA Strand Displacement Circuitry with Self-Resetting Function. J. Am. Chem. Soc. *142*, 21102-21109. 10.1021/jacs.0c09681.
45. Zhang, D.Y., Turberfield, A.J., Yurke, B., and Winfree, E. (2007). Engineering entropy-driven reactions and networks catalyzed by DNA. Science *318*, 1121-1125. 10.1126/science.1148532.
46. Prasad, A., and Alizadeh, E. (2019). Cell Form and Function: Interpreting and Controlling the Shape of Adherent Cells. Trends Biotechnol. *37*, 347-357. 10.1016/j.tibtech.2018.09.007.
47. Caldwell, A.S., Aguado, B.A., and Anseth, K.S. (2020). Designing Microgels for Cell Culture and Controlled Assembly of Tissue Microenvironments. Adv. Funct. Mater. *30*, 1907670. https://doi.org/10.1002/adfm.201907670.